



OPEN ACCESS

Predicting Carbon Sequestration pattern in Casuarina plantation using AANN

G.Arulselvi

Department of Computer Science and Engineering,
Annamalai University, Annamalainagar, Tamilnadu, India

ABSTRACT

Biologic carbon sequestration refers to the assimilation and storage of atmospheric carbon in vegetation, soils, woody products, and aquatic environments. Fluxes of carbon dioxide and other greenhouse gases (GHG) in ecosystems are a function of natural ecosystem processes and anthropogenic activities. Casuarina is an important hardy perennial suitable for coastal areas due to its saline tolerant and drought resistant nature. It is one of the most suited crop for carbon sequestration. Carbon sequestration pattern of perennial vegetation is generally studied using remotely sensed data. In this study, an improved version of remote sensed gross primary production (IRS GPP) model is used for studying carbon sequestration pattern of needle leaf vegetation. This model utilises the features extracted from moderate resolution imaging spectroradiometer (MODIS) data. The vegetation indices namely EVI (Enhanced Vegetation Index), GVM (Global vegetation Moisture index), TRVI (Total ratio vegetation index) and two radiation variables namely LST (Land surface temperature) and Albedo_{NIR} are used to estimate the carbon sequestration potential of casuarina plantation of Cuddalore district of Tamilnadu, India. Classification of carbon sequestration pattern was done using Auto Associative Neural Network (AANN). It classifies the pattern of carbon sequestration of casuarina plantation with an accuracy of 98.63%.

Keywords: Casuarina, MODIS, Gross primary production, Autoassociative neural network.

INTRODUCTION

Casuarina (*Casuarina equisetifolia*) is a drought tolerant, fast growing tree, with wider adaptability. Due to saline tolerant nature, it is commonly grown in the coastal districts of Tamilnadu. It is also grown in sea coast to protect us from natural calamities. It is a good source of raw materials for paper industries as well as for fuel wood in India. Apart from its uses as fuel, wood and raw material for paper industry, it is an efficient carbon and nitrogen fixer and also allows tremendous nutrient return to soil through litter input. Relying on its tolerance to unusually high pH range (8.5-9.5), it has been introduced in Agro forestry system on salt affected and coastal saline soil [25].

Comprehensive report on biomass and productivity of manmade plantations are available. However, information on carbon sequestering potential of casuarinas is scanty, and the GPP estimation for large scale area of casuarina plantation using remote sensing data is not attempted. Hence, the present study was planned to establish the temporal dynamics of carbon sequestering pattern of casuarina plantation in Cuddalore and Perambalur Districts of Tamilnadu, India using multispectral remote sensing data.

The gross primary production (GPP) of an ecosystem represents the gross uptake of carbon dioxide (CO₂) by vegetation for photosynthesis. It is the primary conduit of carbon flux from atmosphere to land and a key source of energy that fuels economies. On the other hand, CO₂ from fossil fuel burning and ecosystem respiration is a major contributor to global warming or greenhouse effect. Fossil fuel burning has perturbed the carbon cycle, and affected the global climate, leading to worldwide research on climate change and the carbon cycle [13], [36]. However, considerable uncertainties still remain regarding the dynamics of carbon fluxes over both short and long time scales and effective strategies are necessary to acquire relevant information about carbon flux processes, to locate and to quantify terrestrial sources and sinks of carbon [26].

As GPP is a measure of carbon uptake by vegetation, an improved knowledge about GPP can provide us a useful measure of the health of ecosystem and the global carbon cycle. Estimating GPP of terrestrial ecosystems has been challenging because of its dependence on a variety of environmental factors [21]. Among the existing methods, the light use efficiency (LUE) model proposed by Monteith has been widely

used [45], [28], [6] to simulate the spatial and temporal dynamics of GPP because of its theoretical basis and practicality [29]. LUE is defined as the amount of carbon uptake per unit of absorbed photosynthetically active radiation (APAR) by photosynthetic biomass. In LUE, it is assumed that

- the ecosystem GPP is directly related to amount of APAR and
- the actual LUE may be lesser than its theoretical value because of environmental stresses such as low temperatures or water deficits [Yuan et al., 2007].

The general form of LUE is:

$$GPP = \epsilon \times FPAR \times PAR \quad (1)$$

$$\epsilon = \epsilon_{max} \times F \quad (2)$$

Where PAR is the incident photo synthetically active radiation ($MJ\ m^{-2}$) per unit time, FPAR is the fraction of incident PAR absorbed by the canopy, max is the potential LUE ($g\ C\ m^{-2}\ MJ^{-1}APAR$) without environment stress, F is a scalar ranging from 0 to 1 representing the reduction of potential LUE under environmental stresses, $FPAR \times PAR$ gives the APAR and $\epsilon_{max} \times F$ gives the realized LUE(ϵ). In recent years, carbon fluxes measured by the eddy covariance (EC) tower sites set up over forest, grasslands, savannas, etc., has provides useful field measurements for us to parameterize and to validate GPP models. Furthermore, it has been shown that combining these EC tower measurements with remotely sensed (RS) data has the potential to enhance modeling of GPP based on LUE. The MODIS-GPP Algorithm [28], Vegetation Photosynthesis Model [45], EC-LUE [48], etc., are some examples of successful application of remote sensing data in GPP modeling. The objective of this study is to develop a solely remote sensing data based GPP prediction model which does not depend on any supplementary meteorological data. Recently developed remote sensing data based GPP prediction model, which does not depend on any supplementary meteorological data efficiently, calculate and the GPP in different forest ecosystem. [Jahan and Gan, 2009] developed the remotely sensed GPP model, using only on four remote sensing variables - two radiation budget variables ($Albedo_{NIR}$ and LST) and two ecosystem variables - Global vegetation moisture index (GVMI) and Enhanced vegetation index (EVI).

$$GPP = K \times GVMI^a \times LST^b \times Albedo_{NIR}^c \times EVI^d \quad (3)$$

where K is a scalar, and a, b, c, d are exponents. The present study is taken up in semiarid casuarina plantation area, and hence, the remote sensing data based GPP prediction model was modified by adding an additional parameter called total ratio vegetation index (TRVI), which was specific for arid and semiarid vegetation. Several machine learning tools such as SVM, RBFNN and AANN have been used for pattern classification studies. The efficiency of this machine learning techniques varies with the nature of study and data available. The uses of these machine learning techniques in the carbon sequestration pattern studies are scanty. Hence, in the carbon sequestration pattern of casuarina plantation is classified using SVM, RBFNN and AANN. These classification tools utilize the vegetation indices calculated from the MODIS imagery.

MATERIALS AND METHODS

Study site and data sets

Study site

The study site is located in the casuarina plantation of Cuddalore and Perambalur Districts of Tamilnadu, India, and occupies an area of 50,000 *ha*. This area lies between $11^{\circ} 15'N$ to $11^{\circ} 43'N$ latitude and $79^{\circ} 16'E$ to $79^{\circ} 44'E$ longitude and the elevation of the study area ranges from 5 to 65 MSL. The year is broadly divisible into two seasons: Dry season (March to September) and Wet season (October to February). Of the total annual rainfall 1012 *cm*, north east monsoon (October-December) accounts for 75% of the rainfall and the remaining 25% of the rainfall occurs during January-September. The mean monthly maximum and minimum temperature ranges are 28 to $44^{\circ} C$ and 22 - $28^{\circ} C$ respectively. The soil is sodic with sandy to silty clay loam texture characterized by unusually high pH (8.5-9.5) indicating poor waterholding capacity to poor permeability.

Remotely sensed data:

For the study site, the 8-day surface reflectance data (MOD09A1, Collection 5) of the four spectral bands, blue, red, NIR (841-875 *nm*), and shortwave infrared (1628-1652 135 *nm*) were collected from 2007 to 2010 and then used to calculate vegetation indices - EVI and GVMI. The other 8-day composite MODIS data sets used in this study include the 1 *km* LST (MOD11A2, collection 5) and 1 *km* GPP product (MOD17A2, Collection 5).

MOD11A2 is retrieved using the Split-Window algorithm and the thermal infra-red bands of MODIS [Wan and Dozier, 1996]. We also collected MODIS albedo product which is produced every 8 days with 16 days of acquisition. The Bidirectional Reflectance Distribution Function (BRDF) coefficients from MCD43A1 were used to calculate the actual albedo for the visible (VIS), NIR and shortwave bands (0.3- 0.7, 0.7-5.0, and 0.3-5.0 μm , respectively) as a function of optical depth, solar zenith angle, band [Schaaf et al., 2002], <http://daac.ornl.gov/MODIS/MODISmenu/MCD43.html>.

We estimated GPP with 1 km resolution which is same as that of MODIS GPP. Since the remotely sensed data are of 1 km (LST, MODIS GPP) and 500 m (reflectance and *albedo*) resolutions, for LST and MODIS GPP, we extracted digital values of a 1-km pixel; while for reflectance and albedo, we used the average value of 2x2 pixels which represents the same 1km x 1km area.

Research methodology

The research approach for casuarina plantation undertaken in this study can be summarized as follows:

1. Selecting EVI, GVMi, Albedo_{NIR}, LST and TRVI as the model predictors and investigating the relationships between these model predictors and GPP.
2. Calibrating GPP using IRS model for the year 2007-2010, and comparing its results with the MODIS GPP product (MODIS-17A2).
3. Calculating the efficiency of AANN for classification of carbon sequestration pattern of casuarina plantation.

IRS-GPP model predictors

Global Vegetation Moisture Index GVMi:

Previous studies have demonstrated the possibility of using NIR and short wave infra-red bands to retrieve leaf and canopy water content (g/m^2) using Landsat-TM data [Hunl and Rock, 1989], hyperspectral data [Serrano et al., 2000], and VEGETATION (VGT) sensor data [2]. Recently, [3], [4] proposed to retrieve equivalent water thickness (EWT) at the canopy level using GVMi from the VGT sensor:

$$GVMi = \frac{(NIR + 0.1) - (SWIR + 0.02)}{(NIR + 0.1) + (SWIR + 0.002)} \quad (4)$$

where NIR and SWIR are reflectance of the rectified NIR band and short wave infrared bands, respectively. [4] tested GVMi in retrieving EWT from four different ecosystems and found that water content retrieved from GVMi was consistent with field measured water content. Other studies also demonstrated the applicability of GVMi in retrieving EWT [Dansan and Bowyer, 2004], [Du et al., 2005]. To incorporate the effect of water stress in the R-GPP model, we used GVMi computed from MODIS reflectance products. In this study, we found that seasonal dynamics of GPP agrees well with GVMi ($R^2 = 0.86$) for the casuarinas plantation Fig. 1(b) and therefore GVMi is selected as a predictor.

When there is sufficient soil moisture (water is not a limiting factor), photosynthesis will probably depend more on temperature which is related to the incoming solar radiation. [Yuan et al., 2007] also reported that GPP is controlled either by air temperature or by soil moisture, whichever is the most limiting.

Near-infrared Albedo ($Albedo_{NIR}$):

Albedo (α), the fraction of incident solar radiation reflected by a surface plays a key role in partitioning the total radiative flux into absorbed, sensible, latent, and reflected fluxes [Bounoun et al., 2000]. The net radiation R_n is given as

$$R_n = \begin{cases} S_{in} - S_{out} + L_{in} - L_{out} \\ S_{in}(1 - \alpha) + L_{in} - L_{out} \end{cases} \quad (5)$$

where S_{in} and S_{out} are the incoming and outgoing solar (shortwave) radiation; L_{in} and L_{out} are the down welling and upwelling longwave radiation at the surface, respectively. *Albedo* influences the radiation absorbed by plant canopies and thereby affects physical and bio-geochemical processes such as photosynthesis, energy balance, evapotranspiration, and respiration [38-41].

Furthermore, surface albedo also affects rainfall, vegetation growth [Bounoua et al., 2000], [Wang and Davidson, 2007] and even droughts that could lead to desertification [Knorr et al., 2001]. The albedo of vegetation, unlike that of bare soil, shows temporal variability due to the seasonal behavior of plant phenology such as green-up, peak greenness, drydown, and senescence. For example, Song [Song, 1998] found that the albedo of a wheat field decreased from the peak green to senescence stage.

Although some previous studies on GPP [Gebremichael and Barros, 2006], [Lchii et al., 2003] used albedo to calculate radiative fluxes, as far we know, none of them reported a direct relationship between NIR albedo and GPP, and most of these models used a constant albedo without considering its temporal variability.

In this study, albedo at the NIR band, $Albedo_{NIR}$ (0.7 to $5\mu m$) has been used because the reflectance of vegetation is very strong at NIR band, and likely because of this reason, it is the most commonly used albedo in ecosystem modeling [37], [10], [23].

Since only 16-day resolution albedo data is available from MODIS, we have used that 16-day albedo product produced every 8 days (e.g., albedo of Date 1 corresponds to average albedo of day 1 to 16 while albedo of date 9 corresponds to average albedo of Date 9 to 24). To estimate the GPP of any 8 day period, we have used $Albedo_{NIR}$ averaged over that particular 8-day and the previous 8-day while the other predictors were averaged over that particular 8-day. For example, to calculate the average GPP of day 9 to 16 (17 to 24), the average albedo of day 1 to 16 (9 to 24) is used while the other predictors were averages of day 9 to 16 (17 to 24). Therefore the R-GPP remains as an 8-day GPP model.

Fig. 2(b) shows that the seasonal dynamics of $Albedo_{NIR}$ and GPP is strongly correlated with each other ($R^2=0.82$) and hence it was selected as a model predictor in IRS model. $Albedo_{NIR}$ gradually increases with the fresh of leaf formation because of the high reflectance of canopy leaves in the NIR band and continues until the peak green stage and then gradually decreases with the senescence of leaves is observed by Wang [38] for a boreal deciduous forest of Saskatchewan, Canada.

Enhanced Vegetation Index (EVI):

EVI produces vegetation signal with improved vegetation monitoring through canopy background and atmospheric corrections [36] as shown in Equation 6. It is more sensitive than the popular normalized difference vegetation index (NDVI) in high biomass regions. EVI has been shown to be a good predictor of growing season GPP for many sites and it was used as a predictor in some previous models [Xiao et al., 2004]. In this study we found that the seasonal dynamics of GPP agrees reasonably well with EVI ($R^2=0.84$) for the casuarina plantation Fig. 1(a) and shows that EVI is selected as a predictor.

$$EVI = G \frac{NIR - RED}{NIR + C_1 RED - C_2 B + L} \quad (6)$$

Land Surface Temperature (LST):

LST is a potential predictor for GPP estimation because it can incorporate the effect of temperature and Vapor pressure density (VPD) on vegetation [Hashimoto et al.,2008]. It is highly correlated with vegetation dynamics [Sun and Kafatos,2007] and is positively correlated with NDVI in high latitudes ([Karnieli et al.,2006]). The slope of LST/NDVI to be related to the evapotranspiration of Soil. Some studies [Yuan et al., 2007], [Sims et al., 2008] reported that photosynthesis is predominantly controlled by temperature only at the beginning and the end of a growing season, but by moisture conditions throughout the growing season. Therefore we used a scaled LST (LSTs) (equ.7) to set GPP to zero when LST is below 0°C.

$$LST_s = \begin{cases} \frac{LST}{LST_{max}}; & \text{when } LST > 0^\circ C \\ 0; & \text{when } LST \leq 0^\circ C \end{cases} \quad (7)$$

where LST is the observed LST and LST_{max} is the maximum LST. In this study LST_{max} is set to 45°C. Fig. 3(a) shows that GPP is strongly correlated with LSTs ($R^2=0.71$). From January to April, GPP increases with increasing LSTs; beyond that it decreases upto July due to high temperature and leaf senescence. The LST start increases again from July due to the onset of southwest monsoon as shown in Fig. 3(a). However, it is also found that GPP does not respond instantaneously to temperature rise during the early growing season. Furthermore, low LSTs during the start and the end of each growing year restricts water and nutrient uptake, and hence, it affects photosynthesis [Sims et al., 2008].

Total ratio vegetation index (TRVI):

In arid and semi-arid regions, soil background has more reflectance in the near infrared (NIR) and red (RED) wavelengths of vegetation. Soil components that affect spectral reflection include colour, roughness and water content. Roughness also has the effect of decreasing reflectance because of an increase in multiple scattering and shading. RED-NIR scattergrams, termed the 'soil line', are used as a reference point in most vegetation studies.

The problem is that real soil surface is not homogeneous and composite of several types. Analysis has shown that for a given soil characteristics, variability in one wavelength is often functionally related to reflectance in another wavelength. Vegetation cover is usually sparse compared to soil background and soil and plant spectral signatures tend to mix non-linearly.

Thus, arid plants tend to lack the strong red edge found in plants of humid regions due to ecological adaptations to the hot desert environment. It is decided to introduce the new vegetation index based on total wavelength (visible and NIR) in the GPP calculation. The total ratio vegetation index (TRVI) is the ratio of NIR and the sum of visible and NIR wavelengths and is calculated using the following equation

$$TRVI = 4 \left[\frac{NIR-RED}{NIR+RED+GR+B} \right] \quad (8)$$

where RED and NIR stands for spectral measurement acquired in the red and near infrared regions, respectively.

For this equation, the normalized difference is divided by the total of visible and near infrared wavelengths. In this equation "4" is the measured reflectance. In fact this equation shows the ratio of the normalized difference of reflectance and measured reflectance of all bands (i.e) the four bands in the multispectral image. [Hadi Fadaei et al., 2012] used TRVI to estimate the stand density of vegetation.

Fig. 2(a) shows that seasonal dynamics of TRVI and GPP is strongly correlated with each other ($R^2=0.88$) and hence TRVI is selected as a model predictor in the present study.

IRS-GPP model development and results

Given that GVMI, EVI, TRVI, Albedo_{NIR} and LSTs are correlated to GPP, we propose a remotely sensed GPP (IRS-GPP) model (9) based on these five RS predictors only,

$$GPP = K \times GVMI^a \times LST^b \times Albedo_{NIR}^c \times EVI^d \times TRVI^e \quad (9)$$

where k is a scalar, and a , b , c , d and e are exponents. These model parameters were calculated using the MODIS data for the study site and a nonlinear optimization scheme, the Generalized Reduced Gradient (GRG2) [Spaulding, 1998]. By GRG2, the optimized values of k , a , b , c , d , e have been found to be 114, 0.885, 1.05, 0.695, 0.933 and 0.01 respectively.

RESULTS AND DISCUSSION

Seasonal dynamics of EVI from eight-day composites of MODIS

The performance of MODIS, EVI changed significantly over time, reaching its peak in early summer and then declining gradually. In the present study the EVI of the casuarina plantation ranged from 0.2 to 0.78, the maximum EVI was noticed in the month of January and the lowest EVI was observed in the peak summer (May) as shown in Fig. 1.

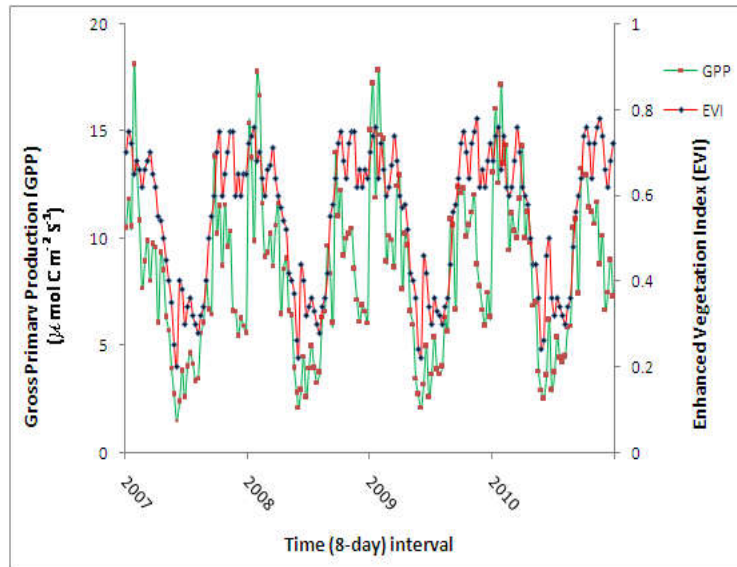
The temporal dynamics of EVI within the plant-growing season is closely correlated to the dynamics of observed GPP. EVI is sensitive to phenological changes in leaf and canopy, and the other factor which affects the EVI is change in photosynthetic active vegetation and nonphotosynthetic vegetation proportions within individual leaves (leaf level), and age of the leaves.

Evergreen needle leaf vegetation consist of leaves with various ages of years. As a needle leaf get old, it changes its size (leaf thickness), dry weight and chlorophyll content. Based on a comparative assessment of needle anatomy of red spruce needle leaf thickness of 1st year leaves is about 1% smaller than that of 2nd year leaves and there is less intracellular air space in the 2nd year leaves .

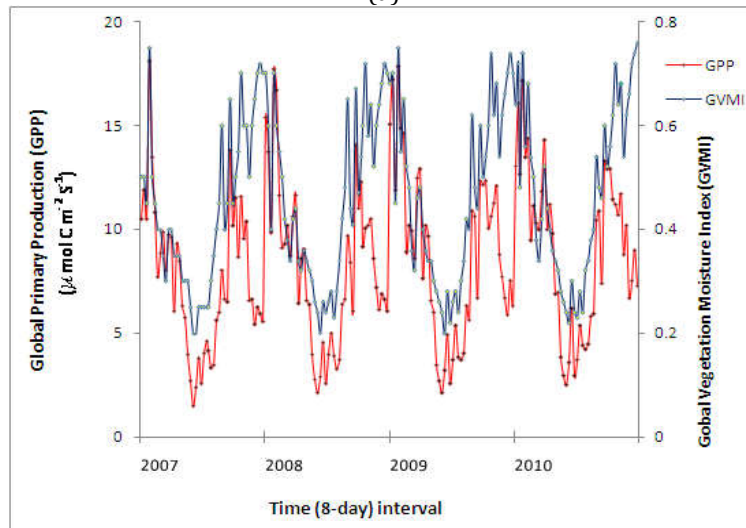
Although chlorophyll concentration may be stable over the seasons, an increase in leaf thickness results in a larger volume of needle leaf, which lead to dilution effect of chlorophyll in the needle leaf. The changes in the leaf size (thickness), intercellular air space, dry weight and distribution effect might together affect reflectance, transmittance and absorption of PAR by needle leaf, for instance, the 2nd year needle leaf have slightly higher reflectance value in the blue band, but little changes of reflectance values in red band in comparison to first year needles. After reaching the peak in early summer, NIR values decline gradually resulting in low EVI value.

Seasonal dynamics of GVMI from eight-day composites of MODIS

The GVMI has distinct seasonal dynamics over the year as shown in Fig. 1(b). High GVMI values in winter and early spring are attributed to increased availability of soil moisture in soil. During the winter and early spring, plant can extract ample quantity of water for its growth, resulting in higher leaf water content. This might be the reason for the high GVMI value during the winter and early spring seasons. As the summer approaches the GVMI starts decreasing due to the reduction in leaf moisture content and leaf maturity. Jahan and Gan [Jahan and Gan, 2011] have established the positive relationship between leaf moisture content and GVMI.



(a)



(b)

Fig. 1: Seasonal Dynamics of (a) Enhanced vegetation index (EVI) with GPP. (b) Global vegetation moisture index (GVMI) with GPP.

Seasonal dynamics of TRVI from eight-day composites of MODIS

Changes in the value of TRVI during the plant growing season is depicted in Fig. 2. In the present study, the TRVI ranged from 0.12 to 0.3, and maximum TRVI is recorded in the month of January. TRVI is also affected by leaf moisture and plant growing season. As the soil moisture declines from January to June, the TRVI also decreases considerably. Vegetation that is dead or stressed reflects more red light and less NIR light. This might be the reason for low TRVI during summer (May-June). Similarly, the TRVI increases as the new leaves are formed, this was clearly noticed in the study from the month of July to December, which coincides with the onset of monsoon rain fall. The lowest TRVI was observed in the month of May-June. A positive correlation (0.84) was noticed between TRVI and GPP.

The present study is conducted in semi-arid region. Generally in semi-arid region, the green vegetation index tends to decrease with low reflecting soil background and the influence of soil background has been found to seriously hamper the assessment and characterisation of vegetation canopy cover [Huete and Jackson, 1987]. Use of this TRVI in the IRS model might have reduced the impact of reflection from soil background.

Seasonal dynamics of Albedo ($Albedo_{NIR}$) from eight-day composites of MODIS

Reflectance of vegetation is very strong at NIR band and likely because of this reason, it is most commonly used in ecosystem modeling. In the present study, the albedo value ranged from 0.14 to 0.3. As that of EVI, and GVMI, albedo value also increased during the new flush formation and in early spring season. The maximum albedo (0.3) was noticed in the month of February and started declining during summer as shown in Fig. 2(b). The lower albedo value of (0.14) was noticed in the month of May. From the month of

June onwards, $Albedo_{NIR}$ gradually increased with the green up of leaves due to the onset of south west monsoon, high reflectance of canopy leaves in NIR band continued until the peak green stage and then gradually decreased with the senescence of leaves as it was observed by Wang [Wang,2005] for boreal deciduous forest of Canada.

Seasonal dynamics of LST from eight-day composites of MODIS

Temperature is an important factor which directly influences the photosynthesis and GPP. In this study the LST ranged from 0.25 to 0.8, from the month of January to April. The LST increased gradually and reached the peak value in the month of May and then declined. The GPP_{obs} increased with increase in LST till April, beyond that GPP decreased as the LST increased. Again from the month of June, LST started declining whereas GPP increased gradually as shown in Fig. 3(a).

Predicted gross primary production from eight-day composites of MODIS

The results from simulations of the IRS model using eight-day composite MODIS data have shown that the IRS model predicts reasonably well the gross primary production of a casuarina plantation. The IRS model overestimated GPP as compared to MODIS GPP as indicated by the slopes of simple linear regression models between IRS model predicted GPP and MODIS GPP as shown in Fig. 3(b). IRS GPP_{pred} (from eight day MODIS composites) was only slightly larger (5%) than MODIS GPP. Performance of all models depends upon input data.

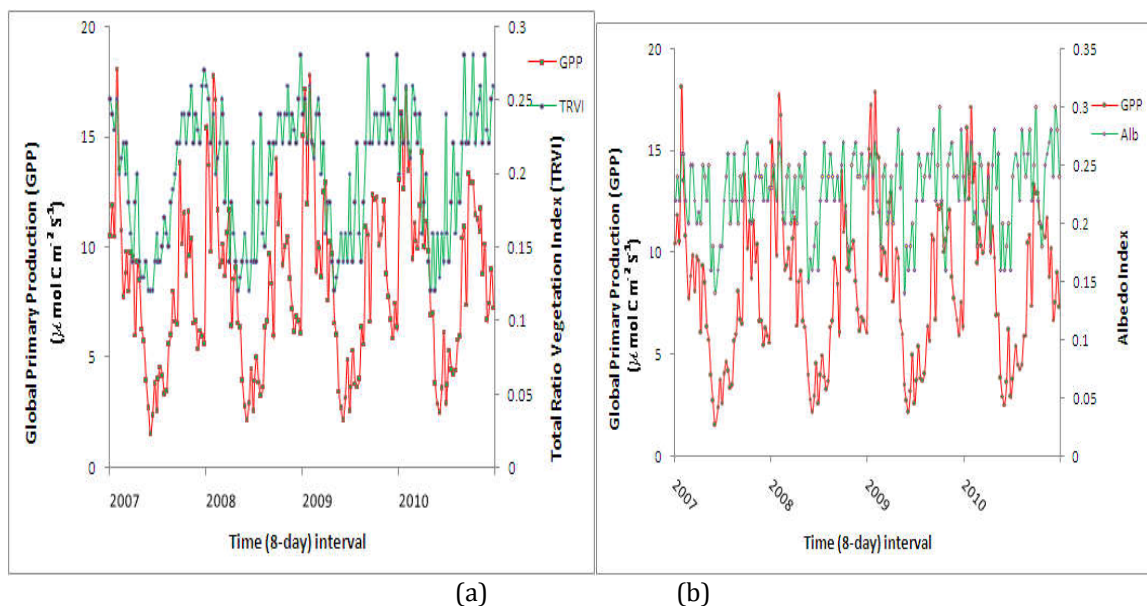
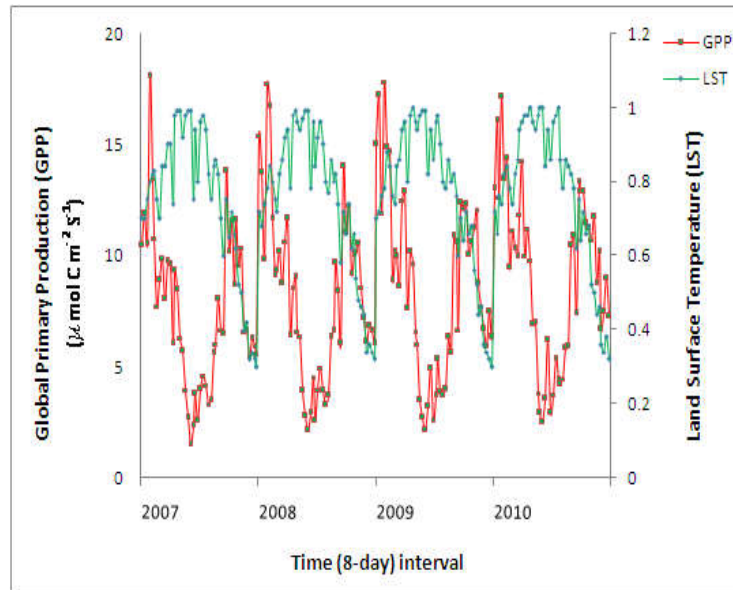


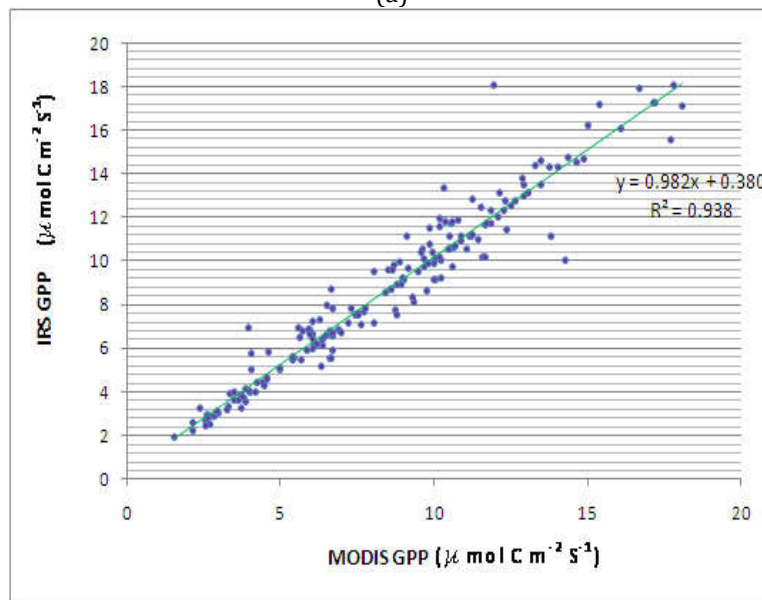
Fig. 2: Seasonal Dynamics of (a) Total ratio vegetation index (TRVI) with GPP. (b) Albedo index with GPP.

For the IRS model, it is largely vegetation indices from eight-day MODIS imagery that affect performance of IRS model. In comparison to other PEM models that employ only NDVI [Running et al., 2000], the IRS model has three simple but innovative features. The first feature is that the IRS model uses an improved vegetation index that is related to vegetation greenness (EVI). The second feature is that the IRS model uses an improved vegetation index that is related to vegetation water content (GVMI) to estimate the effect of water on photosynthesis and the third important feature is vegetation index related to arid and semiarid vegetation (TRVI), which minimize the soil background reflection in the GPP model.

One advantage of using water-related vegetation index in the IRS model is that there is no need for a soil moisture model that is usually driven by very coarse resolution of input datasets (e.g., precipitation, soil texture, and soil depth), which could result in large uncertainty or error in soil moisture. There exist a few water-oriented vegetation indices [Ceccato et al, 2002(a)], [Ceccato et al, 2002(b)], [Xiao et al., 2002], [Maki et al., 2004], and extensive field work is needed to collect seasonal data of leaf and canopy water content, which would help to evaluate those spectral water indices and improve understanding of water-related biophysical processes of leaves over time.



(a)



(b)

Fig. 3: (a) Seasonal Dynamics of LST and GPP. (b) Comparison of IRS GPP with MODIS GPP.

In addition, a comparison between water-related vegetation index and soil moisture data from a soil moisture model should be conducted. Although these two innovative features need to be validated across various biomes through systematic and extensive field measurement and radiative transfer modeling, the IRS model has the potential to improve estimation of seasonal dynamics and interannual variations of gross primary production of arid and semiarid perennial vegetation, in comparison to the other existing PEM models that employ NDVI only.

The IRS model uses the new vegetation index, the total ratio vegetation index which is developed specifically for the arid and semiarid regions to minimize the soil background reflection.

Pattern classification Technique

Use of machine learning techniques for carbon sequestration pattern is an active research area in remote sensing. Recently, non-parametric models, such as neural networks have demonstrated successful performances. In the present study autoassociative neural network (AANN) are used for carbon sequestration pattern classification.

Auto associative Neural Network Models

Autoassociative neural network models are feed forward neural networks performing an identity mapping of the input space, and are used to capture the distribution of the input data [Yegnanarayan and

Kishore, 2002], [Palanivel, 2002]. Limitation of principal component analysis (PCA) to represent an input space using a linear subspace motivated the researchers to investigate a method of projecting the input data onto a non-linear subspace using AANN models. AANN consists of three layers namely input layer, hidden layer and output layer. An AANN is a feed forward network with the desired output being the same as the input vector. Therefore, the number of units in the input and output layers are equal. The number of hidden layers and the number of units in each hidden layer depend on the problem.

A three layer AANN model clusters the input data in the linear subspace, whereas a five layer AANN model captures the non-linear subspace passing through the distribution of the input data. Studies on three layer AANN models show that the non-linear activation function at the hidden units clusters the input data in a linear subspace. Theoretically, it was shown that the weights of the network will produce small errors only for a set of points around the training data. When the constraints of the network are relaxed in terms of layers, the network is able to cluster the input data in the non-linear subspace. Hence, a five layer autoassociative neural network model as shown in Fig. 4 is used to capture the distribution of the feature vectors in our study. Let us consider the five layer AANN model shown in Fig. 4, which has three hidden layers. The processing units in the first and third hidden layers are non-linear, and the units in the second compression/hidden layer can be linear or non-linear. As the error between the actual and the desired output vectors is minimized, the cluster of points in the input space determines the shape of the hyper surface obtained by the projection onto the lower dimensional space. The second and fourth layers of the network have more units than the input layer. The third layer has fewer units than the first or fifth. The activation functions at the second, third and fourth layers are non-linear. The structure of the AANN model used in our study is $5Lu\ 10Nu\ 2Nu\ 10Nu\ 5Lu$, where Lu denotes a linear unit and Nu denotes a non-linear unit. The non-linear output function for each unit is $\tanh(s)$, where s is the activation value of the unit.

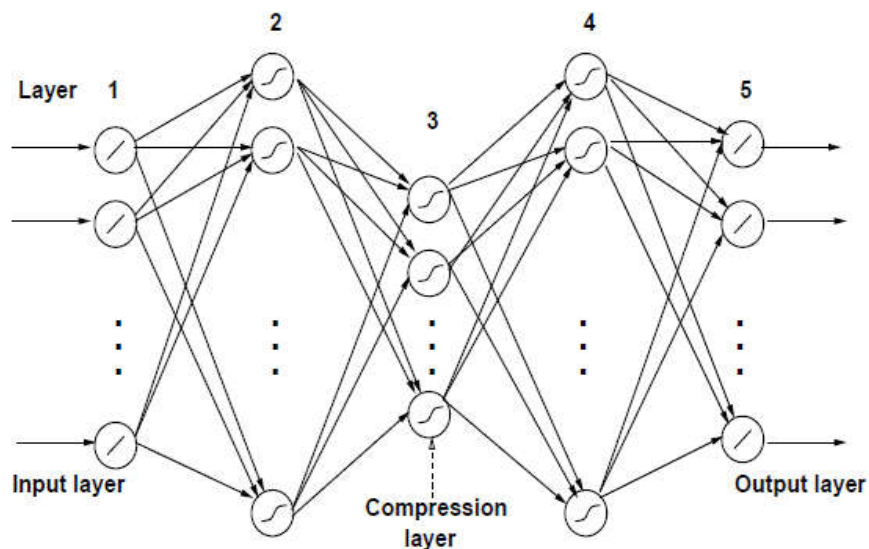


Fig. 4: A five layer AANN model.

The standard back propagation learning algorithm is used to adjust the weights of the network to minimize the mean square error for each feature vector. The AANN captures the distribution of the input data depending on the constraints imposed by the structure of the network, just as the number of mixtures and Gaussian functions do in the case of Gaussian mixture model. The choice of parameters such as feature vectors, initial weights and structure of AANN is not very critical, as variation of these parameters does not affect the performance of the system abruptly [Kishore, 2000].

In order to visualize the distribution better, one can plot the error for each input data point in the form of some probability surface as shown in Fig. 5. The error e_i for the data point i in the input space is plotted

as $p_i = \exp(-e_i/\alpha)$, where α is a constant. Note that p_i is not strictly a probability density function, but we call the resulting surface as probability surface. The plot of the probability surface shows a large amplitude for smaller error e_i , indicating better match of the network for that data point. The constraints imposed by the network can be seen by the shape of the error surface in both the cases. One can use the probability surface to study the characteristics of the distribution of the input data captured by the

network. Ideally, one would like to achieve the best probability surface, best defined in terms of some measure corresponding to a low average error.

During AANN training, the weights of the network are adjusted to minimize the mean square error obtained for each feature vector. If the adjustment of weights is done for all feature vectors once, then the network is said to be trained for one epoch. For successive epochs, the mean square error is averaged over all feature vectors. During the testing phase, the features extracted from the test data are given to the trained AANN model to obtain the average error.

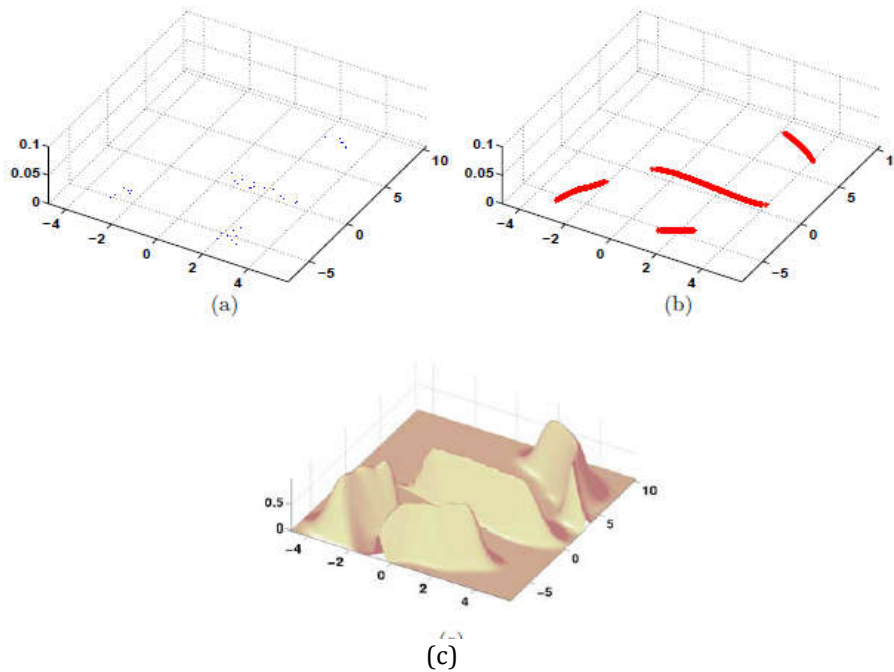


Fig. 5: Distribution capturing ability of AANN model. (a) Artificial 2 dimensional data. (b) 2 dimensional output of AANN model. (c) Probability surfaces realized by the network.

Classification of casuarina plantation using AANN

The AANN was trained with six input features viz., GVMI, LST, $Albedo_{NIR}$, EVI, TRVI and GPP. Depending upon the overall GPP range, the GPP can be classified into three classes such as class 0 (1.0-6.5), class 1 (6.6-12.0) and class 2 (12.1-18.6). The AANN model is trained thrice with these three classes with 100, 400, 700 and 1000 epochs. Then the model was tested using the set of test data, and then the input feature vector is compared with the input to compute the normalized squared error e_k . The normalized squared error (e_k for the feature vector x) is given by

$$e_k = \frac{\|x - o\|^2}{\|x\|^2} \quad (10)$$

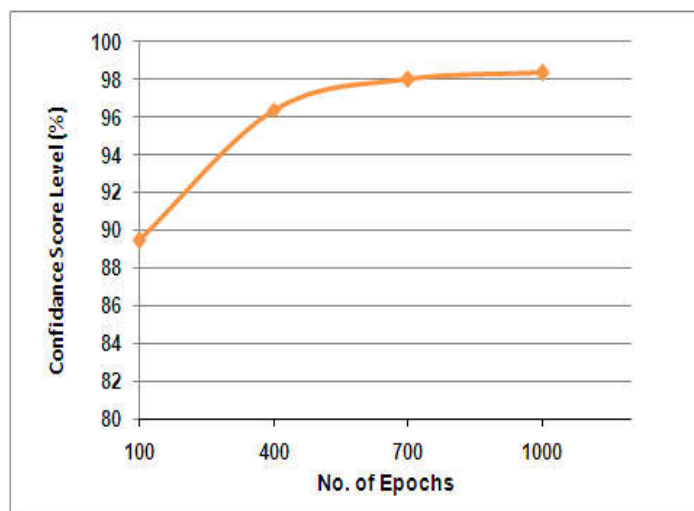
where o is the output vector given by the model. The error e_k is transformed into a confidence score s using

$$s = \exp(-e_k) \quad (11)$$

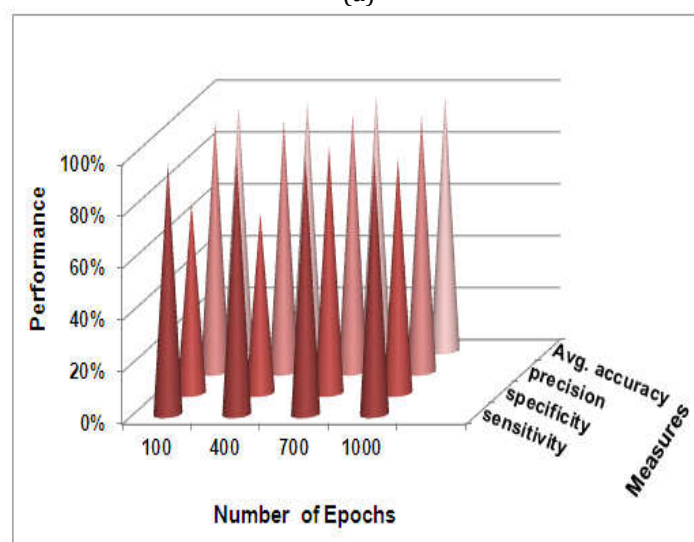
The data set are classified based on the highest confidence score.

In order to test the performance of the AANN model, a set of test data is considered initially. A total dataset of 184 samples are used in our studies. This includes 44 for class 0, 87 for class 1 and 53 for class 2. The six feature vectors of three classes (0, 1, 2) are given as input to the each AANN training and the network is trained for 100, 400, 700 and 1000 epochs. One epoch of training is a single presentation of all the training vectors to the network. The performance of AANN is measured by increasing the epoch from 100 to 400, 700 and 1000. The performance of AANN increased with increasing number of epochs up to 700, beyond that there is no significant change which is clearly depicted in Fig. 6.

Table 1 gives the results of the performance in the form of a confusion matrix for the three different classes such as class 0 (44 instances), class 1 (87 instances) and class 2 (53 instances). The performance measures calculated for the three different classes (class 0, class 1 and class 2) are shown in Table 1, Table 2 and Table 3 and Fig. 4 and Fig. 5.



(a)



(b)

Fig. 6: (a)Effect of epochs on the confidence score. (b) Average performance of AANN for different epochs for each class in casuarina plantation using MODIS.

Class wise performance of AANN for carbon sequestration pattern classification of casuarina plantation using satellite imagery derived vegetation indices (MODIS) are given in Table 1 and Fig. 7(b). The class wise performance of AANN for different epochs are expressed as sensitivity, specificity, precision, F-score and accuracy.

Increase in number of epochs from 100 to 400 increased the sensitivity to 100% in class 0 and 2, where as in class 1 100% sensitivity was achieved only at 700 epochs. In 1000 epochs did not achieved 100% sensitivity in all the three class. 100% specificity was recorded in class 0 and 2 at 700 epochs. In the case of class 1, 100% specificity was achieved at 1000 epochs. However no relationship between number of epochs and specificity variation would be established in this study. As that of specificity, 100% precision was noticed at 700 epochs in class 0 and 2. Where as in class 1 700 epochs achieves the precision of 99%. Increase in the epoch from 100 to 700 increased the F-score and accuracy from 96% to 99% and 93% to 98% in class 0, 97% to 99% and 95% to 99% in class 1 and 97% to 99% and 94% to 98% in class 2 respectively.

Average class performance of AANN for carbon sequestration pattern classification of casuarina plantation using satellite imagery derived vegetation indices (MODIS) are given in Table 2 and Fig. 6(b). The results of the analysis showed that increase in the number of epochs from 100 to 400 will increase the sensitivity from 97% to 99%. Further increase in number of epochs from 400 to 1000 did not increased the sensitivity. No clear trend was noticed with number of epochs and specificity. However 1000 epochs recorded the highest specificity of 90%.

The precision value of 97% was recorded at 100 and 400 epochs. This was increased to 99% at 700 and 1000 epochs. Average accuracy increased with increase in number of epochs from 100 to 700. Both 700 and 1000 epochs recorded the maximum accuracy of 98%.

Performance measures of all classes for carbon sequestration pattern classification of casuarina plantation using satellite imagery derived from vegetation indices are shown in Table 3 and Fig.7(a). The results of the analysis showed that increase in the number of epochs from 100 to 400 increased the sensitivity from 97% to 99%. Further increase in number of epochs did not increase the sensitivity.

With regards to specificity, increase in the number of epochs from 100 to 700 increased the specificity from 78% to 91%. Further increase in number of epochs to 1000 decreased the specificity to 82%.

Precision and accuracy also increased with increased number of epochs from 100 to 700. At 700 epochs precision and F-score achieved the maximum percentage of 99. Further increase in number of epochs (1000), in failed to increase the precision and F-score. However it was mentioned at 99%.

The structure of AANN model plays an important role in capturing the distribution of the feature vectors. The number of units in the third layer (compression layer) determines the number of components captured by the network. The AANN model projects the input vectors onto the subspace spanned by the number of units (nc) in the compression layer. If there are nc units in the compression layer, then the feature vectors are projected onto the subspace spanned by nc components to realize them at the output layer.

The effect of changing the value of nc on the performance of carbon sequestration pattern classification is studied. After some trial and error, the network structure $6L\ 24N\ 4N\ 24N\ 6L$ is obtained. The structure seems to give good performance in terms of classification accuracy. The results are shown in Table 5.

Similarly, the performance is obtained by varying the number of units in the second layer (expansion layer) by keeping the number of units in the compression layer as "4". When the number of units in the expansion layer is changed from 12 to 30, there is no considerable increase in the performance. The performance of carbon sequestration pattern classification in terms of number of units in the expansion layer is shown in Table 5. From the results, it is observed that the overall classification accuracy is 98.63%.

Table 1: Class-wise performance of AANN for carbon sequestration pattern classification of cashew plantation using satellite imagery derived vegetation indices (MODIS).

Class	Epochs	Sensitivity (%)	Specificity (%)	Precision (%)	F-Score (%)	Accuracy (%)
0	100	97.00	60.00	95.00	96.00	93.00
	400	100	50.00	95.00	98.00	95.00
	700	98.00	100	100	99.00	98.00
	1000	98.00	100	100	99.00	98.00
1	100	97.00	86.00	97.00	97.00	95.00
	400	97.00	83.00	97.00	97.00	95.00
	700	100	86.00	99.00	99.00	99.00
	1000	100	71.00	98.00	99.00	98.00
2	100	96.00	75.00	98.00	97.00	94.00
	400	100	75.00	98.00	99.00	98.00
	700	98.00	100	100	99.00	98.00
	1000	98.00	74.31	100	99.00	98.00

Table 2: Average class performance of AANN for carbon sequestration pattern classification of casuarina plantation using satellite imagery derived vegetation indices (MODIS).

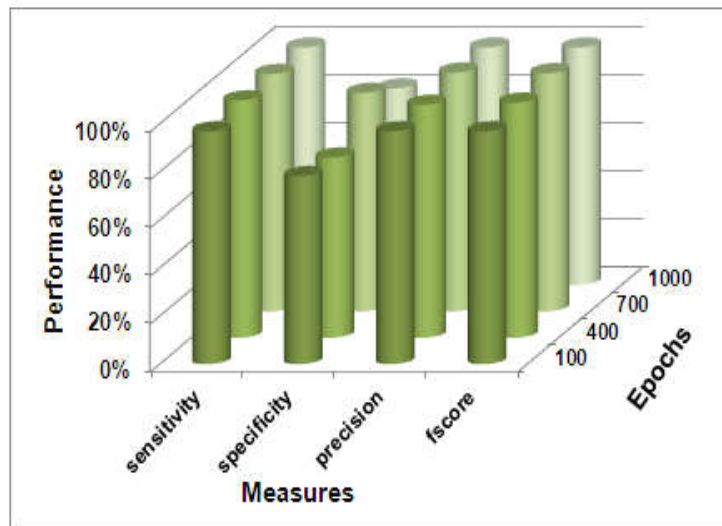
Epochs	Sensitivity (%)	Specificity (%)	Precision (%)	Average Accuracy (%)
100	97.00	74.00	97.00	94.00
400	99.00	69.00	97.00	96.00
700	99.00	75.00	99.00	98.00
1000	99.00	90.00	99.00	98.00

Table 3: Performance measures of all classes for carbon sequestration pattern classification of casuarina plantation using satellite imagery derived vegetation indices.

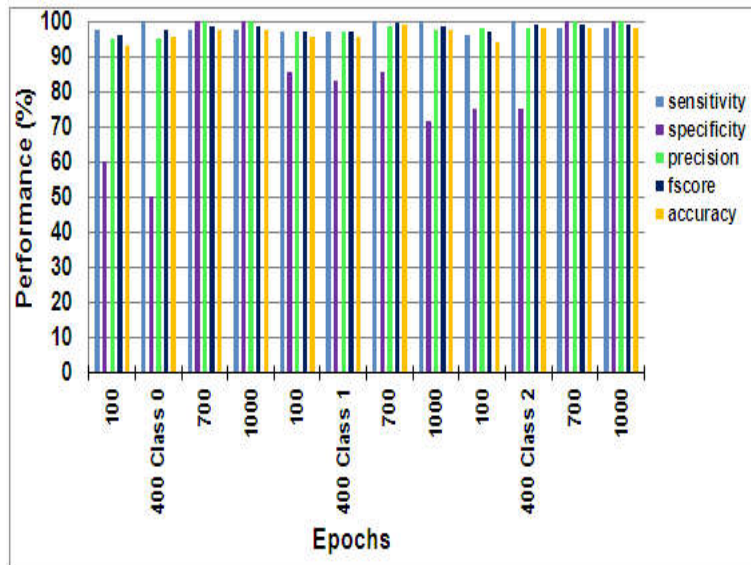
Epochs	Sensitivity (%)	Specificity (%)	Precision (%)	F-Score (%)
100	97.00	78.00	97.00	97.00
400	99.00	75.00	97.00	98.00
700	99.00	91.00	99.00	99.00
1000	99.00	82.00	99.00	99.00

Table 4: Performance of carbon sequestration pattern classification of casuarinas plantation in terms of number of units in the compression layer.

Number of units in the compression layer (n_c)	2	3	4	5
Classification rate (in %)	75.0	92.6	97.88	90.0



(a)



(b)

Fig. 7: ((a) Performance of AANN for different epochs for all classes. (b) Over all performance of AANN for each epochs in casuarina plantation using MODIS.

Table 5: Performance of carbon sequestration pattern classification of casuarinas plantation in terms of number of units in the expansion layer.

Number of units in the expansion layer (n_e)	12	18	24	30
Classification rate (in %)	87.14	92.0	98.56	94.77

CONCLUSION

In this study, the improved remote sensing data based GPP model (IRS), which uses MODIS imagery derived three vegetation indices namely EVI, GVMi and TRVI and two radiation budget variables Albedo_{NIR} and LST for the calculation of GPP using IRS model. The same five features along with GPP is used as input parameter for training and testing the AANN. It classifies the pattern of carbon sequestration of casuarina plantation with an accuracy of 98.63%.

REFERENCES

1. L. Bounoua, G. J. Collatz, S. O. Los, P. J. Sellers, D. A. Dazilich, C. J. Tucker, and D. A. Randall, "Sensitivity of climate to changes in NDVI," *J. of Climate*, vol. 13, pp. 2277–2292, 2000.
2. P. Ceccato, S. Flasse, S. Tarantola, S. Jacquemoud, and J. M. Gregoire, "Detecting vegetation leaf water content using reflectance in the optical domain," *Remote Sensing of Environment*, vol. 77, pp. 22–33, 2001.
3. P. Ceccato, S. Flasse, S. Tarantola, S. Jacquemoud, and J. M. Gregoire, "Detecting vegetation leaf water content using reflectance in the optical domain," *Remote Sensing of Environment*, vol. 77, pp. 22–33, 2001.
4. P. Ceccato, S. Flasse, and J. M. Gregoire, "Designing a spectral index to estimate vegetation water content from remote sensing data part 2. validation and applications," *Remote Sensing of Environment*, vol. 82, pp. 198–207, 2002(a).
5. P. Ceccato, N. Gobron, S. Flasse, B. Pinty, and S. Tarantola, "Designing a spectral index to estimate vegetation water content from remote sensing data: Part 1 theoretical approach," *Remote Sensing of Environment*, vol. 82, pp. 188–197, 2002(b).
6. N. C. Coops, R. H. Waring, and B. E. Law, "Assessing the past and future distribution and productivity of ponderosa pine in the pacific northwest using a process model, 3-PG," *Ecological Modelling*, vol. 183, pp. 107–124, 2005.
7. F. M. Danson and P. Bowyer, "Estimating live fuel moisture content from remotely sensed reflectance," *Remote Sensing of Environment*, vol. 92, pp. 30–321, 2004.
8. X. Du, S. Wang, and Y. Zhou, "Monitoring and spatio-temporal evolution researching on vegetation leaf water in china," vol. 4, pp. 2365–2368, 2005.
9. M. Gebremichael and E. P. Barros, "Evaluation of MODIS gross primary productivity (GPP) in tropical monsoon region," *Remote Sensing of Environment*, vol. 100, pp. 150–166, 2006.

10. Ghulam, Q. Qin, and Z. Zhan, "Designing of the perpendicular drought index," *Remote Sensing of Environment*, vol. 52, pp. 1045–1052, 2007.
11. Hadi Fadaei, Rikie Suzuki, Tetsuro Sakai, and Kiyoshi Torii, "A proposed new vegetation index, the total ratio vegetation index (TRVI), for arid and semi-arid regions," *International Archives Photogrammetry, Remote Sensing and Spatial Information Sciences*, vol. XXXIX-B8, 2012.
12. H. Hashimoto, J. L. Dungan, M. A. White, F. Yang, A. R. Michaelis, S. W. Running, and R. R. Nemani, "Satellite-based estimation of surface vapor pressure deficits using MODIS land surface temperature data," *Remote Sensing of Environment*, vol. 112, pp. 142–155, 2008.
13. F. A. Heinsch, M. Zhao, S. W. Running, J. S. Kimball, R. R. Nemani, K. J. Davis, P. V. Bolstad, B. D. Cook, A. R. Desai, D. M. Ricciuto, B. E. Law, W. C. Oechel, H. Kwon, H. Luo, S. C. Wofsy, A. L. Dunn, J. W. Munger, D. D. Baldocchi, L. Xu, D. Y. Hollinger, A. D. Richardson, P. C. Stoy, M. B. S. Siqueira, R. K. Monson, S. P. Burns, and L. B. Flanagan, "Evaluation of remote sensing based terrestrial production from MODIS using AmeriFlux eddy tower flux network observations," *IEEE Trans. Geosci. Remote Sens.*, vol. 44, pp. 1908–1925, 2006.
14. R. Huete and R. D. Jackson, "Suitability of spectral indices for evaluating vegetation characteristics on arid range lands," *Remote Sensing of Environment*, vol. 25, pp. 89–105, 1987.
15. N. Jahan and T. Y. Gan, "Modeling gross primary production of deciduous forest using remotely sensed radiation and ecosystem variables," *Journal of Geophysical Research*, vol. 114, pp. G04026, 2009.
16. N. Jahan and T. Y. Gan, "Modeling vegetation-climate relationship in a central mixed wood forest region of Alberta using normalized difference and enhanced vegetation indices," *Journal of Geophysical Research*, vol. 32, pp. 313–335, 2011.
17. Karnieli, M. Bayasgalan, Y. Bayasgalan, N. Agam, S. Khudulmur, and C. J. Tucker, "Comments on the use of the vegetation health index over Mongolia," *Int. J. remote sensing*, vol. 27, pp. 2017–2024, 2006.
18. S. P. Kishore, *Speaker verification using autoassociative neural networks model*, M. S. thesis, Department of Computer Science and Engg., Indian Institute of Technology, Madras, 2000.
19. W. Knorr, K. G. Schnitzler, and Y. Govaerts, "The role of bright desert regions in shaping North African climate," *Geophys. Res. Lett.*, vol. 28, pp. 3489–3492, 2001.
20. K. Lchii, Y. Matsui, K. Murakami, T. Mukai, Y. Yamguchi, and K. Ogawa, "A simple global carbon and energy coupled cycled model for global warming simulation: sensitivity to the light saturation effect," *Tellus*, vol. 55, pp. 676–691, 2003.
21. Makela, M. Pulkkinen, P. Kolari, F. Lagergren, P. A. Lindroth, D. Loustau, E. Nikinmaa, T. Vesala, and P. Hari, "Developing an empirical model of standard GPP with the LUE approach: analysis of eddy covariance data at five contrasting coniferous sites in Europe," *Global Change Biol.*, vol. 14, pp. 92–108, 2008.
22. M. Maki, M. Ishihara, and M. Tamura, "Estimation of leaf water status to monitor the risk of forest fires by using remotely sensed data," *Remote Sensing of Environment*, vol. 90, pp. 441–450, 2004.
23. S. V. Ollinger, A. D. Richardson, M. E. Martin, D. Y. Hollinger, S. E. Frolking, P. B. Reich, L. C. Plourde, G. G. Katul, J. W. Munger, R. Oren, M. L. Smith, K. T. Paw, P. V. Bolstad, B. D. Cook, M. C. Day, T. A. Martin, R. K. Monson, and H. P. Schmid, "Canopy nitrogen, carbon assimilation, and albedo in temperate and boreal forest: Functional relations and potential climate feedbacks," *PNAS*, vol. 105, pp. 19366–19341, 2008.
24. S. Palanivel, *Person authentication using speech, face and visual speech*, Ph.D. thesis, Department of Computer Science and Engg., Indian Institute of Technology, Madras, 2004.
25. K. S. Parihar and B. S. Rana, "Management practices in agroforestry," In: *Technical report on Biennial workshop on All India Coordinated Research Project on Agroforestry. (I.C.A.R.)*, pp. 40–44, Mar. 1999
26. F. Rahman, D. A. Sims, V. D. Cordova, and B. Z. El-Masri, "Potential of MODIS EVI and surface temperature for directly estimating per-pixel ecosystem C fluxes," *Geophys. Res. Lett.*, vol. 32, no. L19404, pp. doi:10.1029/2005GL024127, 2005
27. Ruimy, G. Dedieu, and B. Saugier, "TURC: a diagnostic model of continental gross primary productivity and net primary productivity," *Global Biogeochemical Cycles*, vol. 10, pp. 269–285, 1996
28. S. W. Running, P. E. Thornton, R. Nemani, and J. M. Glassy, "Global terrestrial gross and net primary productivity from the Earth Observing stem. In O. E. Sala, R. B. Jackson, H. A. Mooney and R. W. Howarth (Eds.)," pp. 44–57, 2000.
29. S. W. Running, R. R. Nemani, F. A. Heinsch, M. Zhao, M. Reeves, and H. Hashimoto, "A continuous satellite-derived measure of global terrestrial primary production," *Bioscience*, vol. 54, pp. 547–560, 2004.
30. B. Schaaf, F. Gao, A. H. Strahler, W. Lucht, X. Li, T. Tsang, N. C. Strugnell, X. Zhang, Y. Jin, J. P. Muller, P. Lewis, M. Barnsley, P. Hobson, M. Disney, G. Roberts, M. Dunderdale, C. Doll, R. d'Entremont, B. Hu, S. Liang, J. Privette, and D. Roy, "First operational BRDF, albedo nadir reflectance products from MODIS," *Remote Sensing of Environment*, vol. 83, pp. 135–148, 2002.
31. L. Serrano, J. A. Gamon, and J. Penuelas, "Estimation of canopy photosynthetic and nonphotosynthetic components from spectral transmittance," *Ecology*, vol. 81, pp. 3149–3162, 2000.
32. A. Sims, A. F. Rahman, V. D. Cordova, B. Z. El-Masri, D. D. Baldocchi, L. B. Flanagan, A. H. Goldstein, D. Y. Hollinger, L. Misson, R. K. Monson, W. C. Oechel, H. P. Schmid, S. C. Wofsy, and L. Xu, "A new model of gross primary productivity for North American ecosystems based solely on the enhanced vegetation index and land surface temperature from MODIS," *Remote Sensing of Environment*, vol. 112, pp. 1633–1644, 2008.
33. J. Song, "Diurnal asymmetry in surface albedo," *Agricultural and Forest Meteorology*, vol. 92, pp. 181–189, 1998.
34. K. A. Spaulding, "Neural metamorphic optimization algorithms," 1998.
35. Sun and M. Kafatos, "Note on the NDVI-LST relationship and the use of temperature related drought indices over north America," *Geophys. Res. Lett.*, vol. 34, pp. L24406, 2007.

36. S. Urbanski, C. Barford, S. Wofsy, C. Kucharik, E. Pyle, J. Budney, K. McKain, D. Fitzjarrald, M. Czikowsky, and J. W. Munger, "Factors controlling CO₂ exchange on time scales from hourly to decadal at Harvard Forest," *Journal of Geophysical Research*, vol. 112, no. G02020, pp. doi:10.1029/2006JG000293, 2007.
37. Z.Wan and J. Dozier, "A generalized split-window algorithm for retrieving landsurface temperature from space," *IEEE Trans. Geosci. Remote Sens.*, vol. 34, pp. 892-905, 1996.
38. S. Wang, R. F. Grant, D. L. Versegny, and T. A. Black, "Modelling plant carbon and nitrogen dynamics of a boreal aspen forest in CLASS - The Canadian Land Surface Scheme," *Ecological Modelling*, vol. 142, pp. 135-154, 2001.
39. S.Wang, R. F. Grant, D. L. Versegny, and T. A. Black, "Modelling carbon dynamics of boreal forest ecosystems using the Canadian Land Surface Scheme," *Climatic Change*, vol. 55, pp. 451-477, 2002(a).
40. S. Wang, W. Chen, and J. Cihlar, "New calculation methods of diurnal distributions of solar radiation and its interception by canopy over complex terrain," *Ecological Modelling*, vol. 155, pp. 191-204, 2002(b).
41. S. Wang, "Dynamics of surface albedo of a boreal forest and its simulation," *Ecological Modelling*, vol. 183, pp. 477-494, 2005.
42. S. Wang and A. Davidson, "Impact of climate variations on surface albedo of a temperate grassland," *Agricultural and Forest Meteorology*, pp. 133-142, 2007.
43. R. H. Waring, N. C. Coops, W. Fan, and J. M. Nightingale, "MODIS Enhanced Vegetation Index predicts tree species richness across forested ecoregions in the contiguous U.S.A.," *Remote Sensing of Environment*, vol. 103, pp. 218-226, 2006.
44. X. Xiao, S. Boles, S. Froking, W. Salas, B. Moore, C. Li, L. He, and R. Zhao, "Observation of flooding and rice transplanting of paddy rice fields at the site to landscape scales in China using VEGETATION sensor data," *International Journal of Remote Sensing*, vol. 23, pp. 3009-3022, 2002.
45. X. Xiao, D. Hollinger, J. D. Aber, M. Goltz, E. A. Davidson, Q. Zhang, and I. Berrien Moore, "Satellite-based modeling of gross primary production in an evergreen needleleaf forest," *Remote Sensing of Environment*, vol. 89, pp. 519-534, 2004.
46. Yegnanarayana and S. P. Kishore, "AANN: An alternative to GMM for pattern recognition," *IEEE Trans. Neural Networks*, vol. 15, pp. 459-469, Apr. 2002.
47. W. Yuan, S. Liu, G. Zhou, L. L. Tieszen, D. Baldocchi, C. Bernhofer, H. Gholz, A. H. Goldstein, M. L. Goulden, D. Y. Hollinger, Y. Hu, B. E. Law, P. C. Stoy, T. Vesala, and S. C. Wofsy, "Deriving a light use efficiency model from eddy covariance flux data for predicting daily gross primary production across biomes," *Agricultural and Forest Meteorology*, vol. 143, pp. 189-207, 2007.